

Content-based onboard compression for remote sensing images



Cuiping Shi^{a,b}, Junping Zhang^{a,*}, Ye Zhang^a

^a Department of Information Engineering, Harbin Institute of Technology, Harbin 150001, China

^b Department of Communication Engineering, Qiqihar University, Qiqihar 161000, China

ARTICLE INFO

Article history:

Received 7 August 2015

Received in revised form

8 December 2015

Accepted 17 January 2016

Available online 8 February 2016

Keywords:

Onboard compression

Content-based

Adaptive scanning

Remote sensing image

Binary tree coding

ABSTRACT

New-generation instruments on spacecraft are collecting a large amount of information at an increasing rate, which makes the onboard data compression a challenging task. Moreover, existing compression methods usually scan an image in a fixed way without considering the content of the image, which makes the performance improvements of these methods often marginal at best. In this paper, we present a novel, content-based, adaptive scanning (CAS) scheme for onboard compression. For a remote sensing image, first, the wavelet transform is performed. Second, an adaptive scanning method is proposed, which can provide different scanning orders among and within subbands, respectively. The former aims at organizing the codestream according to the importance of subbands, and the latter focuses on preserving the texture information as much as possible. Finally, the binary tree codec is utilized to code the 1-D coefficient array after scanning. Experimental results demonstrate that compared with other scan-based compression methods, including CCSDS, JPEG2000, and even the state-of-the-art adaptive binary tree coding (BTCA), the proposed compression method can effectively improve the coding performance. In addition, the method does not use entropy coding or any complicated components, which makes it extremely suitable for onboard compression.

© 2016 Elsevier B.V. All rights reserved.

1. Introduction

Along with the development of sensor technology, the spatial and spectral resolutions of remote sensing images have been greatly improved, which enhances the applicability of remote sensing images. However, there is cost of the large amount of data in that the data storage and transmission of onboard equipment is highly difficult. To alleviate this issue, a compression method with high coding performance and low complexity is very desirable. In general, the compression of remote sensing images involves some traditional compression schemes, such as EZW [1], SPIHT [2], SPECK [3], and JPEG2000 [4]. These compression schemes can effectively compress natural images because the details of natural images are often limited. After the discrete wavelet transform (DWT), a compact representation can be obtained. However, compared with natural images, remote sensing images have their own unique characteristics. They usually contain a large number of ground objects, which leads to a considerable number of details, such as geometric information, edge and texture information, and outlines of small targets. As a result, it is difficult to achieve high coding performance for remote sensing images because the coefficients of the high frequency subbands are still very large after the DWT. In recent years, some compression schemes specifically

designed for remote sensing images have been proposed [5–8]. These compression schemes compress remote sensing images from several aspects, such as oriented wavelet transform (OWT) or sparse representation. Moreover, several machine learning methods are also adopted [9–12]. However, for onboard compression, the compression method should also be of low complexity. Therefore, some additional onboard compression methods have been proposed [13–19]. These onboard compression methods are designed based on several aspects, such as prediction, vector quantization, or distributed source coding (DSC). Because remote sensing images are often captured by sensors in a push-broom fashion and are quite large, the scan-based approach is also very desirable when handling onboard data [20].

In 2006, a scan-based method using JPEG2000 with incrementally acquired data was proposed [21]. However, the cost of the high-quality coding performance of JPEG2000 is its high complexity. The Consultative Committee for Space Data Systems (CCSDS) published a recommended standard for onboard image compression, and published the CCSDS-IDC Blue Book [22] for specific compression algorithms in 2005 and Green Book [23] for guidance of the IDC Recommendation in 2007. The standard of CCSDS is a scan-based algorithm, but it does not allow for interactive decoding. Furthermore, the level of DWT is fixed to three. In 2009, [14] presented some prominent extensions to the CCSDS, which allowed any number of wavelet decomposition levels and supported several forms of remote sensing image coding.

* Corresponding author.

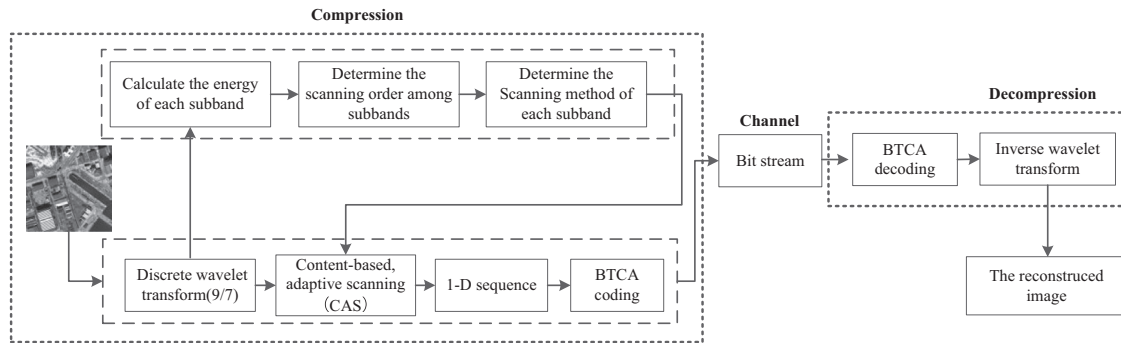


Fig. 1 The overall framework of the proposed compression method.

However, all of these methods are based on fixed scanning, which do not take the content of an image into consideration.

In 2012, the state-of-the-art compression method based on scanning for remote sensing images, known as adaptive binary tree coding (BTCA), was proposed [20]. The main concept of this method is that for a binary tree, it scans the significant nodes and their brothers before other nodes. This method can significantly improve the coding performance.

Although the process of BTCA is somehow related to the content of the image, it does not take an important procedure into account, i.e., the process of scanning an image. The BTCA directly converts a 2-D transformed image into a 1-D sequence by morton scanning. However, different remote sensing images are of different contents. In other words, for different remote sensing images, the spatial distribution of important coefficients is different. Thus, from the perspective of scanning, the morton scan may not be suitable for all images. In addition, remote sensing images are often rich in details, which leads to substantial amounts of information left in high frequency subbands after the wavelet transform. Moreover, for a given level of decomposition, the energy of HL, LH, and HH may be quite different. Therefore, the scanning order among these subbands is very important.

Focusing on the problems mentioned above, in this paper, a low-complexity, content-based, adaptive scanning (CAS) approach for onboard compression is proposed. The content of an image can be described from different perspectives, such as color, texture, shape and structure. In this paper, the content of an image refers to the energy distribution of different wavelet subbands. For different images, the direction information is different and can be reflected from the energy distribution of subbands. If the direction information can be utilized to determine the scanning order and scanning method, then those coefficients that can make a greater contribution to the reconstructed image can be preserved more effectively.

The paper is organized as follows. In Section 2, the novel content-based adaptive scanning scheme for the remote sensing image is designed. Firstly, some common scanning strategies are analyzed. Then, a detailed description of the proposed CAS-based compression scheme is provided. Finally, the computational complexity of the proposed method is analyzed. Section 3 describes the binary tree codes. Section 4 overviews some quality evaluation indices used in this paper. In Section 5, we present some numerical experiments and demonstrate the validity of the proposed method. Finally, a discussion of the results and conclusions is provided in Section 6.

2. Proposed content-based adaptive scanning method

The overall framework of the proposed content-based adaptive scanning compression method is shown in Fig. 1.

For the proposed method, the scanning order among the subbands is determined by the content of the image, and the scanning method within a subband depends on the characteristics of the current subband. When the scanning of a transformed image is finished, a 1-D coefficient sequence is generated. Finally, the binary tree codec is exploited to encode the 1-D coefficient sequence. The proposed method is not complicated, but it can provide a high-quality coding performance.

2.1. Features of the remote sensing images

Based on the type of remote sensor, remote sensing images can be classified into different categories, including optical images, synthetic aperture radar (SAR) images, infrared images, multi-spectral images and hyperspectral images [15]. For each type of remote sensing image, some compression methods have been proposed according to its features [24–29]. Optical remote sensing images¹ are often characterized by a high degree of randomness, weak local correlation, and multiple small targets [18], which result in a larger amount of non-zero coefficients in high frequency subbands after the wavelet transform. Four images, including two well-known natural images (Airplane, Goldhill) and two remote-sensing images (Europa3 and Ocean in Fig. 2), are chosen to compare the energy distribution of high frequency subbands (5-level DWT by the 9/7 biorthogonal filters); the result of comparison is shown in Fig. 3.

It has been demonstrated in Fig. 3 that the energy of almost every high-frequency subband of the remote sensing images is higher than that of the natural images. In addition, for these remote sensing images, the energy fluctuation among subbands is greater than that of natural images. This suggests that for remote sensing images, a different scanning order among subbands will have a greater impact on the coding performance. Therefore, the coding performance improvement is usually very marginal by using the traditional compression methods because they do not take the characteristics of the remote sensing images into consideration. To address this problem, developing a compression method that applies to remote sensing images is ideal.

2.2. Analysis of some common scanning strategies

For an image X , with a size of $M \times N$, the process of scanning the image can be defined as a bijection f from a closed interval $[1, 2, \dots, M \times N]$ to the set of ordered pairs $\{(i, j) : 1 \leq i \leq M, 1 \leq j \leq N\}$, where the latter set represents the locations in the image [30]. After scanning, the two-dimensional (2-D) image is converted to a one-dimensional (1-D) sequence that

¹ For convenience, the optical remote sensing image in this paper is referred to as a remote sensing image hereafter.

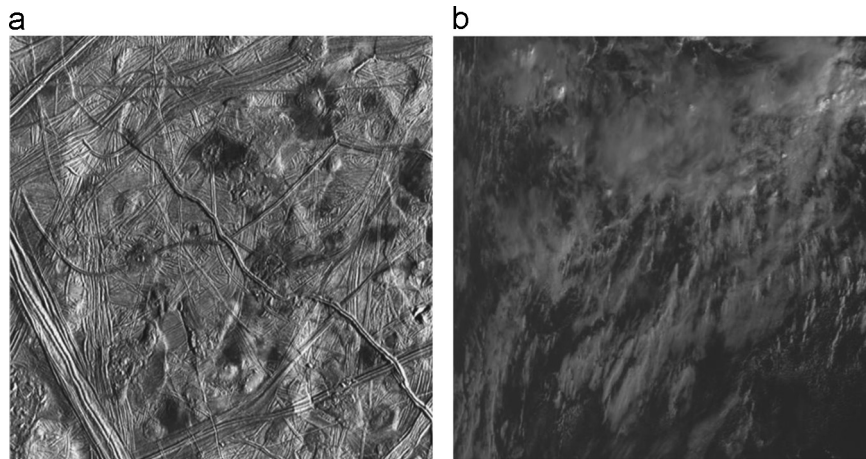


Fig. 2. Remote sensing images used to compare the energy of high frequency subbands with that of natural images: (a) Europa3 (512 × 512); (b) Ocean_2 kb1 (512 × 512).

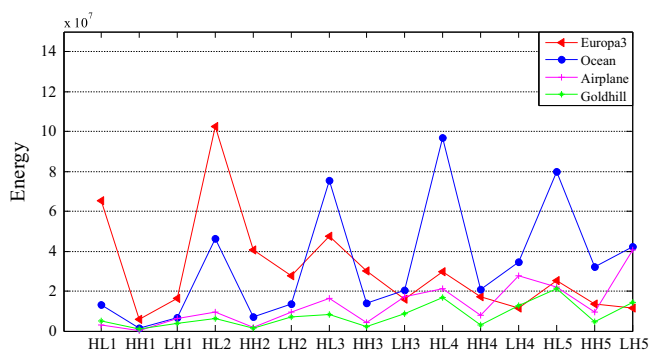


Fig. 3. The energy of each high-frequency subband for the four test images.

can be recorded as $[X_{f(1)}, X_{f(2)}, \dots, X_{f(MN)}]$. Various scanning strategies, in fact, are bijection functions f that are of different definitions. Once the definition of function f is given, then the process of compressing a 2-D image becomes a process of compressing a 1-D sequence $\tilde{X} = [X_{f(1)}, X_{f(2)}, \dots, X_{f(MN)}]$.

Generally, a 2-D image can be converted into a 1-D sequence by certain canonical scanning strategies, such as raster scanning, zigzag scanning, morton scanning and Hilbert scanning. Different scanning strategies are suitable for different applications. Take an 8×8 array for example; the scanning processes of these scanning strategies are shown in Fig. 4(a)–(d), respectively.

The context-based predictive techniques, which are typically designed for lossless compression, commonly adopt raster scanning but, in rare cases, employ Hilbert scanning [31]. A previous study [30] noted that predictive-based coders with the raster scan usually outperform those coders with the Hilbert scan. The spatial correlation of an image makes the raster scan intrinsically superior to other scanning techniques when the predictive technique is used.

Transform-based coding methods have been widely used for image compression. Zigzag scanning can efficiently group the coefficients when the DCT transform is used. Thus, zigzag scans are usually employed in the application of video compression, such as MPEG2 and H.264. However, as shown in Fig. 4(b), the zigzag scan is essentially a type of “line” scan, i.e., instead of representing some insignificant “block”, it can only represent an insignificant “line”. For a wavelet-transformed image, there could be many insignificant “blocks” in the wavelet domain. If these insignificant “blocks” can be scanned properly, the coding performance would be improved. Especially in the case of using a tree to organize coefficients, the “descendant” relationship of the tree will make these zero “blocks” more important than those zero “lines” in the wavelet domain.

Both morton scanning and Hilbert scanning can scan an image in a manner of “blocks”. Some classic coding algorithms, such as EZW and SPIHT, are designed based on morton scanning. However, although morton scanning can scan an image in a manner of “blocks”, it does not take the characteristics of the wavelet subbands into consideration. For a remote sensing image, considerable information still exists in high frequency subbands after the wavelet transform. The fixed scanning mode may affect the coding performance.

The Hilbert scan is a well-known space-filling curve that visits every point of the grid exactly once. The canonical Hilbert scan provides a specific scanning orientation with respect to the coordinate frame and is denoted as the scan of order n . Fig. 4(d) shows the canonical Hilbert scan when $n = 3$. Hilbert scanning was once considered to be the best scanning method for compressing images because of its advantages of “clustering” or “locality preserving” properties, which can be utilized to provide better compression performance. In some applications, it seems more applicable than morton scanning. However, similar to morton scans, Hilbert scans still do not take the characteristics of the wavelet subbands into account.

2.3. Content-based adaptive scanning (CAS)

For an original image, after the wavelet transform, the coefficients that were scanned first are encoded in priority. Typically, the organization of the codestream is based on the scanning order. This indicates that the codestream of the coefficients that were scanned first is in front of the entire codestream. As a result, this part of the codestream will be decoded and displayed if necessary. Therefore, at the same bit rate, different scanning orders can lead to different qualities of the reconstructed image, which makes the scanning order very important. If the coefficients that make a greater contribution to image reconstruction can be scanned first, then the quality of the reconstructed image will be improved, especially in low bit rate applications.

Based on the discussion in Section 2.2, for the scanning of a transformed image, the “block” scanning method is more appropriate. A question then arises: for a remote sensing image, what is a proper “block” scanning method? In addition, compared to a natural image, the high frequency subbands of a remote sensing image usually include more abundant information, which makes the scanning method choice have a greater impact on the quality of the reconstructed image. Therefore, determining the scanning order among subbands also needs to be considered.

In this paper, we present a novel, content-based, adaptive scanning (CAS) scheme for the compression of remote sensing

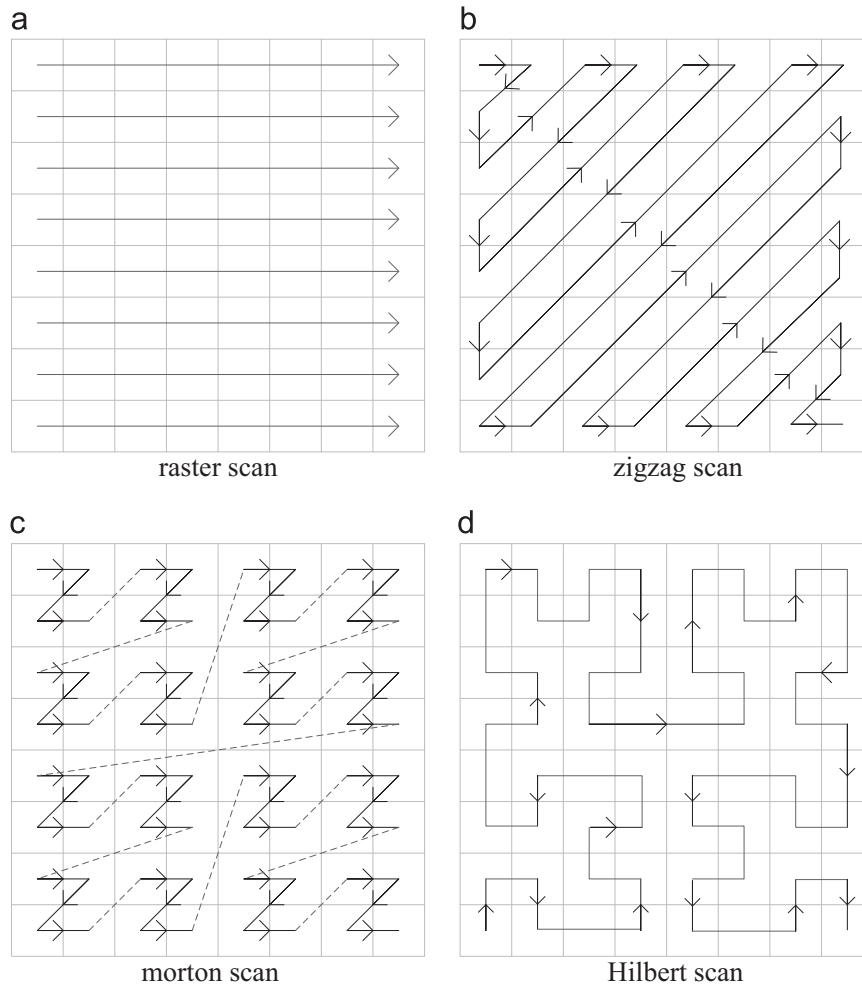


Fig. 4. The scanning processes of some canonical scanning strategies.

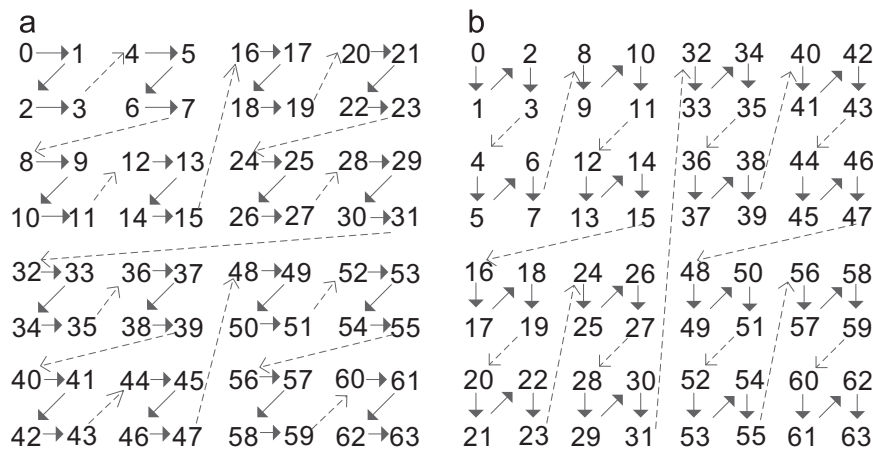


Fig. 5. The “horizontal z-scan” method and the “vertical z-scan” method: (a) the “horizontal z-scan” method is used for the subbands that contain more horizontal information; (b) the “vertical z-scan” method is used for the subbands that contain more vertical information.

images, which determines the scanning method and scanning order based on the image content. The procedure of the CAS is shown in Algorithm 1.

It has been demonstrated that from Algorithm 1, the CAS method is performed by two steps. Firstly, after the wavelet-transform, the energy of each subband is calculated, and the

scanning order among subbands is determined by their energy in descending order. The purpose of doing so is to scan important subbands as soon as possible. Secondly, for the scanning within a subband, we take the characteristics of subbands into consideration. Because the horizontal subbands reflect the information of an image in the horizontal direction, we adopt the “horizontal z-scan”

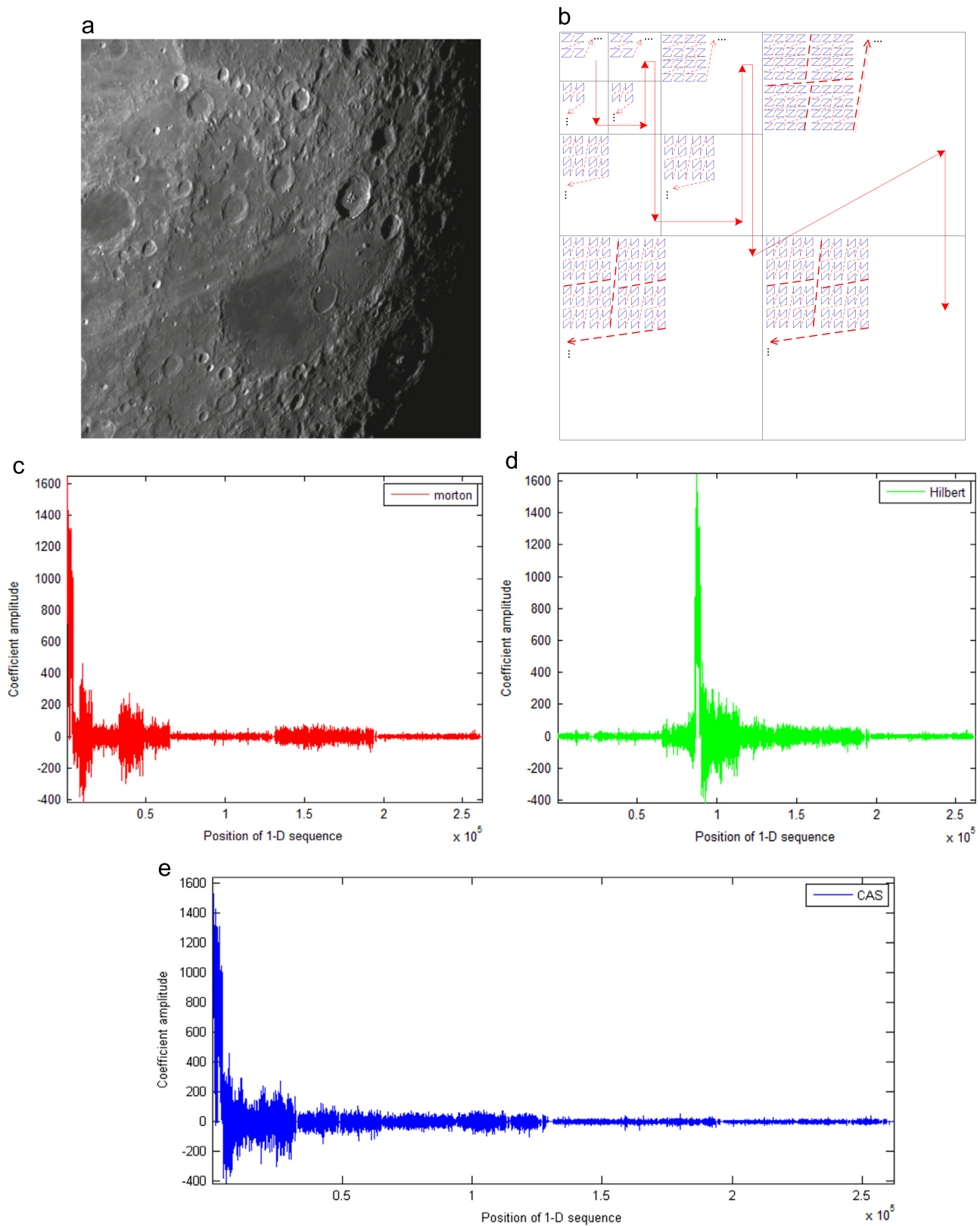


Fig. 6. The original image and its process of scanning: (a) Lunar (8 bit, 512×512); (b) CAS of the transformed image of (a); (c) The 1-D sequence obtained by the morton scan; (d) The 1-D sequence obtained by the Hilbert scan; (e) The 1-D sequence obtained by the proposed CAS scan.

as the scanning method. Similarly, because the vertical subbands represent the vertical information of an image, if the scanning method can perform along the vertical direction, coding

performance should be improved. In this paper, the “vertical z-scan” method is conducted to the vertical subbands. The “horizontal z-scan” method and the “vertical z-scan” methods are

shown in Fig. 5(a) and (b), respectively. For the diagonal subbands, the scanning method depends on the image itself, i.e., if the horizontal information of an image is much greater than the vertical information in the current wavelet level, then the “horizontal z-scan” method is adopted. In the opposite case, the “vertical z-scan” method is adopted.

Algorithm 1. The process of CAS of a transformed image.

Input: A transformed image X , the level of decomposition is J .

- Calculate the energy of each subband, and represent it as $E_{\lambda,\theta}$.

λ -Scale ($m = 1, 2, \dots, J$), θ -Direction ($d = 1, 2, 3, 4$). ‘1’ represents the lowest frequency subband, ‘2’ represents the horizontal direction, ‘3’ represents the diagonal direction, and ‘4’ represents the vertical direction, respectively.

$$E_{\lambda,\theta} = \frac{1}{RC} \sum_{ij}^{R,C} X(\lambda, \theta)(i,j)^2$$

R and C are the number of rows and columns of the current subband $X(\lambda, \theta)$, respectively; $X(\lambda, \theta)(i,j)$ represents the coefficient of the current subband located in (i,j) .

- Determine the scanning order among all the subbands according to their energy.
- **For** each subband $X(\lambda, \theta)$,
 1. If the subband is the lowest frequency subband or horizontal subband, the “horizontal z-scan” is adopted.
 2. If the direction of the subband is vertical, the “vertical z-scan” is exploited.
 3. If the direction of the subband is diagonal, then the scanning method depends on the horizontal subband and vertical subband of this level.

- ① If $E_{\lambda,2} \geq E_{\lambda,4}$, the “horizontal z-scan” is performed to this subband. ② If $E_{\lambda,2} < E_{\lambda,4}$, the “vertical z-scan” is performed to this subband.

End

Output: 1-D sequence of coefficients generated by scanning the 2-D transformed image.

We give an example of the CAS method. The original image is shown in Fig. 6(a). Suppose the level of wavelet decomposition is 3. Based on the process described in algorithm 1, the energy of each subband is calculated; the results are tabulated in Table 1 (In Table 1, the ‘sub’ represents the ‘subband’). According to Table 1, the scanning order among subbands are determined, i.e., LL₃, LH₃, HH₃, HL₃, LH₂, HH₂, HL₂, LH₁, HL₁, and HH₁. Then, for each subband, the scanning method depends on the characteristics of the subband. The “horizontal z-scan” method is used for LL₃, HL₃, HL₂, and HL₁. The “vertical z-scan” method is used for LH₃, LH₂, and LH₁. In Table 1, it can be observed that the vertical information is much greater than the horizontal information for each level of the transformed image. Therefore, for all the diagonal subbands, i.e., HH₃, HH₂, and HH₁, the “vertical z-scan” method is used for scanning. The process of scanning is shown in Fig. 6(b). Finally, the 1-D sequence is obtained. Fig. 6(c)–(e) show the 1-D sequences

Table 1
The energy of each subband of the transformed image ($\times 10^9$).

Sub	Energy	Sub	Energy	Sub	Energy	Sub	Energy
LL ₃	2.2772	HL ₃	0.0038	HH ₃	0.0071	LH ₃	0.0232
–	–	HL ₂	0.0032	HH ₂	0.0039	LH ₂	0.0219
–	–	HL ₁	0.0011	HH ₁	0.0006	LH ₁	0.0079

generated by morton scanning, Hilbert scanning and the proposed CAS method, respectively.

From Fig. 6(c)–(e), we can see that the proposed CAS method can place those important coefficients in front of the 1-D sequence as much as possible, which helps to improve the coding performance.

2.4. Computational complexity

Compared with the BTCA method, the proposed CAS method does not have additional computational cost during the scanning process. The additional computational cost occurs during the determination of the scanning order prior to scanning.

Suppose the size of an image is $M \times N$, and the level of wavelet decomposition is J ; then there are $3J+1$ subbands. Based on Algorithm 1, $C_M = M \times N + (3J+1)$, $C_A = M \times N - 1$, and $C_C = J$, where the subscripts M, A and C represent multiplication, addition, and comparison, respectively. It should be noted in Algorithm 1, the square calculation in the multiplication operation is the main work when calculating the energy of the subbands. In fact, the square calculation can be realized by a shift operation on the hardware for faster speed. Therefore, the additional computational cost is notably small.

2.5. Time complexity

For convenience, we assume the number of rows and columns of the transformed image is the same, i.e., $M = N$.

If the BTCA method is adopted, then there are 2^{2N} nodes at the bottom of the binary tree, and the height of the binary tree is $H_B = \log_2(2^{2N}) + 1 = 2N + 1$. When an upper level node of the tree is constructed, it requires a comparison with its two children. Therefore, the total comparison time for constructing a binary tree is

$$T_{BC} = 2^{2N} \left(\frac{1}{2} + \frac{1}{2^2} + \dots + \frac{1}{2^{H_B-1}} \right) = 2^{2N} - 1 \quad (1)$$

Following the comparison, time is required to traverse these nodes of the binary tree. Suppose the total traversal time is represented as T_{BT} ; then the encoding time of the BTCA can be recorded as

$$T_B = T_{BC} + T_{BT} = (2^{2N} - 1) + T_{BT} \quad (2)$$

Many compression methods that are commonly used are based on quadtree. To identify the maximum magnitude of all possible descendants, a quadtree needs to be constructed in each subband. For the highest resolution subband, there are $2^{2N}/4$ coefficients, so the comparison time for constructing a quadtree in this subband is $2^{2N}/4 - 1$. Suppose the level of wavelet decomposition is J (Typically, $J = 5$); then the total comparison time for constructing the quadtree is

$$T_{QC} = 3 \times \left[\left(\frac{2^{2N}}{4} - 1 \right) + \left(\frac{2^{2N}}{4^2} - 1 \right) + \dots + \left(\frac{2^{2N}}{4^J} - 1 \right) \right] \approx 2^{2N} - 3J \quad (3)$$

If the total traversal time is represented as T_{QT} , then the total encoding time based on the quadtree can be calculated as

$$T_Q = T_{QC} + T_{QT} \approx (2^{2N} - 3J) + T_{QT} \quad (4)$$

From the above analysis, we can see that the comparison time T_{BC} during the construction of the binary tree is nearly equal to the comparison time T_{QC} of the quadtree. Thus, the total encoding time of the binary tree and quadtree mainly depend on the traversal time T_{BT} and T_{QT} , respectively.

For a given transformed image, the number of nodes of the binary tree is $N_B = 2^{2N} + 2^{2N} - 1$, and the number of nodes of the quadtree is $N_Q = 2^{2N} + 2^{2N}/4 + 2^{2N}/4^2$. Obviously, N_B is bigger than N_Q . This means that for binary tree coding, the traversal time is longer than that of the quadtree, although each node does need to be traversed.

For the proposed CAS method, based on the analysis in Section 2.4, compared with the BTCA method, the additional computational time T_0 is

$$T_0 = C_M + C_A + C_c = 2N^2 + 4J \quad (5)$$

Therefore, the total encoding time of the proposed CAS method T_C is

$$T_C = T_B + T_0 = (2^{2N} - 1 + T_{BT}) + 2N^2 + 4J \quad (6)$$

For the encoding of a binary tree, the main works focus on the scanning of those nodes, i.e., the traversal time T_{BT} is far greater than the time of constructing a binary tree T_{BC} . This implies the fact that the total encoding time of the proposed CAS method is close to that of the BTCA method.

2.6. The overhead of bits

In the proposed CAS method, the side information, including the scanning order among the subbands and the scanning method of those diagonal subbands, is also encoded in the bitstream.

For the $3J+1$ subbands, only $3J+1$ integers are needed to represent the scanning order among the subbands. In this paper, the determination order of those subbands is recorded according to LL_j , HL_i , HH_i , and LH_i ($i=J, J-1, \dots, 1$). J integers are needed to represent the scanning methods of those diagonal subbands; the determination order of those diagonal subbands is recorded according to HH_i ($i=J, J-1, \dots, 1$). Here, 0 is used to represent the “horizontal z-scan” and 1 is used to represent the “vertical z-scan”. Therefore, the total cost of the side information is $(3J+1)+J=4J+1$.

We take the image in Fig. 6(a) as an example. Based on Table 1 and Algorithm 1, the scanning order among the subbands are 1, 4, 3, 2, 7, 6, 5, 9, 10, 8, and the scanning methods of diagonal subbands are 1, 1, 1. Thus, the total cost of side information is $10+3=13$. Because the size of the ‘lunar’ is 512×512 , the overhead bits would be approximately 0.0049% of the overall bits. It is worthy to note that the overhead cost only depends on the level of wavelet decomposition. That is, if the size of the image is larger or the bit depth is greater than 8 bit, then the proportion of overhead bits would be smaller. Moreover, if entropy encoding is used for these overhead bits, the overhead cost would be further reduced. Based on the analysis above, the overhead bits of the CAS method are extremely small and can be negligible.

3. Binary tree coding

Most of the embedded coding methods are based on quadtree decomposition, such as EZW, SPIHT and SPECK. However, Shaffer et al. noted that the coding method based on binary tree decomposition is more efficient and simpler than that based on quadtree decomposition [32]. In empirical comparisons, binary tree coding shows an approximately 25% space utilization improvement over quadtree-based coding.

The state-of-the-art compression approach based on binary trees has been previously proposed [20] while utilizing the findings that the wavelet coefficients on the edges are often significant and that the magnitudes of the wavelet coefficients around the edges are often too large too; thus, a new method called adaptive binary tree coding (BTCA) was developed. BTCA is extremely suitable for the compression of remote sensing images because it can preserve the details as much as possible. In this paper, the BTCA is adopted as the embedded codec.

For a given node, the process of binary tree coding (BTC) is described in Algorithm 2. Suppose D represents the bottom level

of the tree, then the process of BTCA can be described by Algorithm 3.

For the embedded codec BTCA, the decoding process is the reverse process of the encoding. Thus, it does not need any extra bits as overhead information. In addition, it can be observed from Fig. 1 that the proposed CAS scheme only works in the process of encoding and is not needed in the decoder. Therefore, it does not affect the decoding speed.

Algorithm 2. : The process of binary tree coding for a given node.

Input: Γ represents a binary tree, and i is the index of the node of the binary tree. T_k represents the current threshold.

Initialization: $T_0 = 2^{\lfloor \log_2 \Gamma(1) \rfloor}$, and $T_k = T_0/2^k$.

- If $\Gamma(i)$ has been coded with a significantly larger threshold, i.e., $\Gamma(i) \geq T_{k-1}$, then
 - If $\Gamma(i)$ is not in the bottom level of the binary tree, code the two children of $\Gamma(i)$, else the sign of $\Gamma(i)$ is coded.
- If $\Gamma(i)$ has a significant parent, and the brother of $\Gamma(i)$ is insignificant, then
 - If $\Gamma(i)$ is not in the bottom level of the binary tree, code the two children of $\Gamma(i)$, else the sign of $\Gamma(i)$ is coded.
- If $\Gamma(i) \geq T_k$
 - If $\Gamma(i)$ is not in the bottom level of the binary tree, code the two children of $\Gamma(i)$, and add a ‘1’ before the codestream. Else the sign of $\Gamma(i)$ is coded, and add a ‘1’ before the codestream.
- Else

‘0’ is output.

Output: The codestream of the subtree whose root is the node $\Gamma(i)$.

Algorithm 3. : The process of BTCA.

Input: T_k is the threshold.

Initialization: $d = D$. While ($d > 1$)

- {
- For $i = \sum_{j=0}^{d-1} 2^j + 1$ to $\sum_{j=0}^d 2^j$
- Let $ct = \{\}$. If $\Gamma(i) \geq T_{k-1}$

If $\Gamma(i)$ is on the left of its brother, then $ct = \text{Algorithm2}(\Gamma, i+1, T_k)$;

Else

$ct = \text{Algorithm2}(\Gamma, i-1, T_k)$.

• $code = \{code, ct\}$.

• $d = d - 1$.

Output: The codestream of the bit plane for the given threshold T_k .

4. The quality evaluation index

To evaluate the proposed compression method comprehensively, we choose PSNR (peak signal-to-noise ratio, dB) and MAE (mean absolute error) as evaluation indices, respectively.

Suppose f and \hat{f} are the original image and the reconstructed image, respectively. The size of the image is $M \times N$. L represents the possible maximum value of the image. Thus, PSNR can be calculated as follows.

$$PSNR = 10 \log_{10} \frac{L^2}{\|f - \hat{f}\|_2} \quad (7)$$

The MAE can be represented as follows.

$$MAE = \frac{1}{MN} \sum |f - \hat{f}| \quad (8)$$

5. Experiment and results

To verify the coding performance of the proposed compression method for remote sensing images, several experiments are implemented. The results of the proposed method are compared with those of other scan-based compression algorithms.

5.1. Satellite images from different sensors

To demonstrate the efficiency of the proposed CAS-based compression method, several test remote sensing images acquired by different sensors are chosen in the experiments. Most are high-resolution images.

Some test images are from CCSDS reference test image sets [33]. The CCSDS reference image set includes a variety of space imaging instrument data, such as solar, stellar, planetary, earth observations and radar. In this image set, “europa3”, “coastal-b1”, “ocean_2kb1”, “pleiades_portdebouc_pan” and “p160_b_f” are chosen. We crop the left upper of these images to a size of 512×512 for comparison under the same condition. Moreover, to fully verify the effectiveness of the proposed compression method, two other remote sensing images are chosen. “pavia” is derived from an image acquired by the QuickBird Sensor over Pavia, northern Italy, which has a resolution of 0.6 m. “houston” is derived from an image acquired by the WorldView–2

Sensor over Houston, TX, USA in 2013, which has a resolution of 0.5 m. The sizes of “pavia” and “houston” are 512×512 . “europa3” and “ocean_2kb1” are shown in Fig. 2(a) and Fig. 2(b), respectively. The rest of the test images are shown in Fig. 7. The bit depth and data source of all the test images are listed in Table 2.

5.2. Experiment results and discussion

In the experiments, these images are all decomposed by five-level 9/7-tap bi-orthogonal wavelet filters. The PSNRs and MAEs at different bit rates of the proposed CAS-based compression methods are compared with those of the other scan-based algorithms, such as SPIHT, SPECK, CCSDS, JPEG2000, and BTCA, respectively.

The results of PSNR and MAE of the proposed method without entropy coding and the other five algorithms at different bit rates are tabulated in Tables 3–5 and Tables 6–8, respectively. These tables are all shown in Appendix A. The results are evaluated at six bit rates, namely, 0.0313 bpp, 0.0625 bpp, 0.125 bpp, 0.5 bpp, 1 bpp, and 1.2 bpp.

Table 2
List of test images.

Image	Bit depth (bpp)	Source
europa3	8	Galileo Image from Europa-NASA
coastal-b1	8	Landsat-NASA
ocean_2kb1	10	NOAA Polar Orbiter (AVHRR)- NOAA
pavia	11	QuickBird (0.6 m)
houston	11	WorldView–2 Sensor(0.5 m)
pleiades1	12	Simulated PLEIADES-CNES
pleiades2	12	Simulated PLEIADES-CNES
p160_b_f	16	Picard Imager (IAS)-CNRS

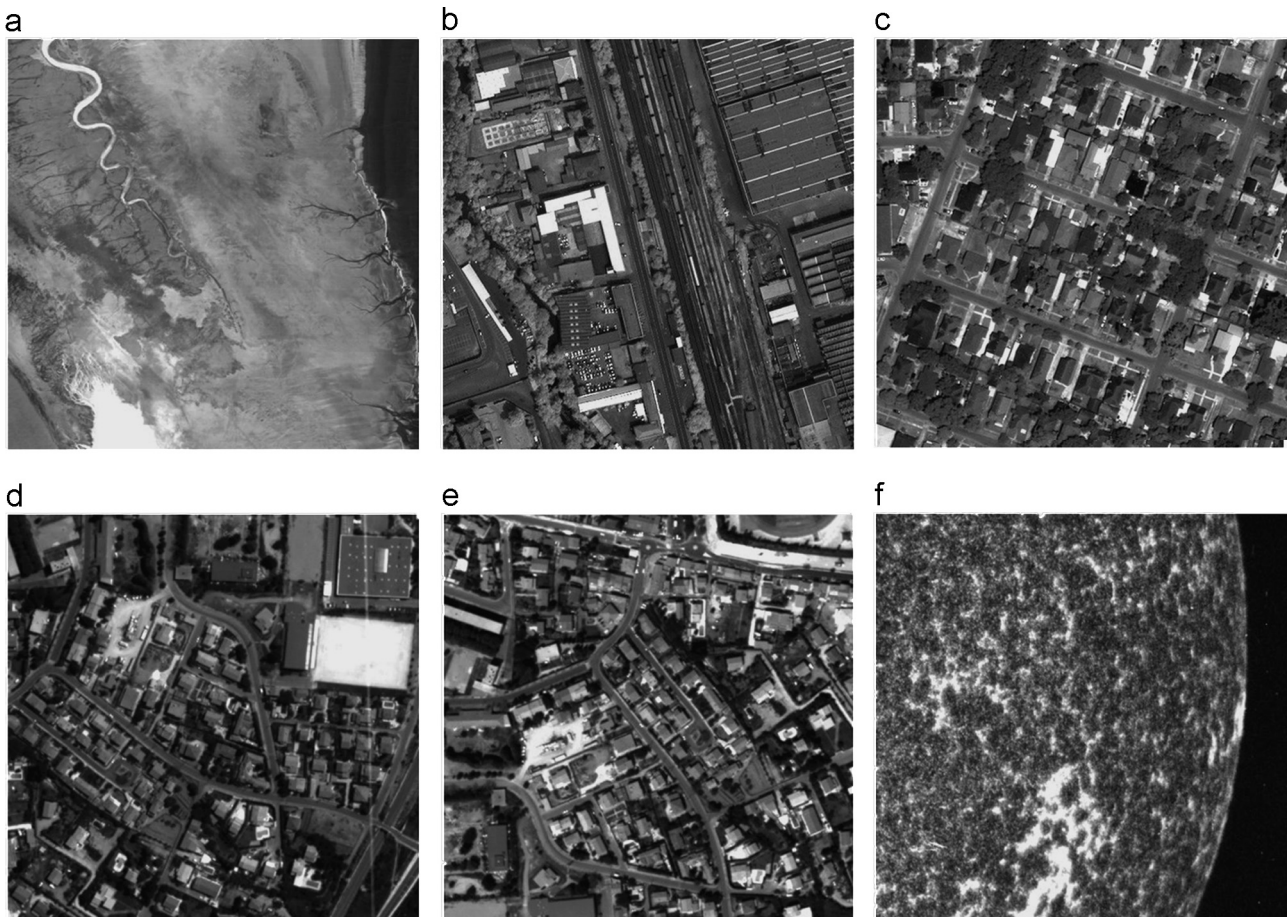


Fig. 7. Parts of the remote sensing images used in the experiment: (a) coastal-b1; (b) pavia; (c) houston; (d) pleiades1; (e) pleiades2; (f) p160_b_f.

From the Tables 3–5, we observe that when the bit rate is less than or equal to 0.125bpp, the PSNR results of CCSDS are the worst. This is because for the CCSDS, the level of the wavelet transform is fixed to three, which limits its coding performance to some extent, especially in the case of low bit rates. JPEG2000 consists of two encoding stages, i.e., tier–1 and tier–2 coding, respectively. After the wavelet transform, the transformed subbands are divided into equal-size coding blocks. To minimize the MSE for the desired bit rate, a rate-distortion optimization process is performed between the tier–1 and tier–2 stages. In addition, some other sophisticated components, such as context modeling, are also adopted for helping achieve a good coding performance. However, the high performance has the cost of high complexity. Compared with BTCA, the PSNR results of SPIHT and SPECK are all lower at these given bit rates. The reason is that the coding method based on binary tree decomposition is more efficient than that based on quad-tree decomposition. For the proposed CAS-based compression method, the PSNR results are all the highest compared with the other scan-based compression methods at all given bit rates, including the BTCA. The proposed CAS-based method takes the scanning order among subbands and the scanning strategy within a subband into consideration simultaneously, which ensures those important coefficients can be scanned first. Therefore, the proposed CAS-based compression method can provide a better coding performance. It is worth noting that the proposed method does not adopt entropy coding, however, the coding performance is still superior to other algorithms with entropy coding, such as JPEG2000. This further illustrates the effectiveness of the proposed method.

Tables 6–8 list the MAE results of the proposed CAS-based compression method and the other five compression methods. Based on the aforementioned analysis, the proposed compression method is still superior to the other methods. When the bit rate is very low, the coding performance of CCSDS is reduced drastically. This situation becomes more evident when the bit depth of the image is very large. For example, for the test images of “pleiades2” or “p160_b_f”, the MAE of the CCSDS is far greater than that of the other compression methods at 0.0313bpp. At the same bit rate, the greater bit depth of the image yields a better compression ratio. For the JPEG2000, some sophisticated components, such as context modeling and rate-distortion optimization, can help achieve a good coding performance. However, the coding performance is still worse than the proposed compression method without entropy coding.

Based on the above analysis, we can conclude that compared with other scan-based methods, the proposed CAS-based compression method can provide a better coding performance. Moreover, it also works well when the bit rate is very low.

6. Conclusions

In this paper, we proposed a novel content-based onboard compression method for remote sensing images. The proposed method

simultaneously considers the scanning order among subbands and the scanning method within a subband. Firstly, the scanning order among subbands is determined according to their energy in descending order. Secondly, the scanning method within a subband is designed based on the characteristics of the subband. Finally, the binary tree codec is exploited to code the generated 1-D sequence of coefficients after scanning. The experimental results validate the proposed method.

The content-based onboard compression method is specifically designed for space data systems. This work is significant because it can effectively improve the coding performance, and can work very well even when the bit rate is very low. Moreover, the proposed compression method does not adopt any sophisticated component; the main work is to compare the value of two numbers, so it is of very low complexity. Therefore, it is very suitable for hardware implementation. For onboard compression, undoubtedly, the work is very meaningful and can be applied to the Space Data Systems.

Multiband images are also highly common in remote sensing applications. For multiband images, e.g., multispectral or hyperspectral images, compared with spatial correlation, the spectral correlation must be considered. However, it is a problem for the proposed method to effectively allocate bit rates across the transformed bands. If a traditional bit allocation method is simply applied, then many details of the remote sensing image will be lost. Therefore, for the multiband image, a specialized bit allocation method that considers the unique characteristics of remote sensing images is more favorable. How to design such a bit allocation method while reducing the complexity of the algorithm as much as possible is an issue worthy of studying. We plan to study this issue in future work.

Acknowledgments

The authors would like to thank the handling editor and the anonymous reviewers for their careful reading and helpful remarks, which have contributed in improving the quality of this paper. This paper is supported in part by the National Natural Science Foundation of China (61271348), and in part by the Prophase Cultivation Project of Technology Achievements Industrialization of Universities in Heilongjiang Province of China under Grant 1254CGZH04.

Appendix A

A.1 The comparison of PSNR results.

See Table 3, Table 4, Table 5.

A.2 The comparison of MAE results.

See Table 6, Table 7, Table 8.

Table 3
PSNR (dB) for the proposed CAS-based compression method and other scan-based compression methods.

Image	0.0313 bpp						0.0625 bpp					
	SPIHT	SPECK	CCSDS	J2K	BTCA	CAS-based	SPIHT	SPECK	CCSDS	J2K	BTCA	CAS-based
europa3	15.46	16.40	9.20	16.21	16.45	16.47	16.55	17.05	14.28	16.91	17.20	17.22
coastal-b1	25.69	32.02	16.52	31.56	32.13	32.15	31.64	33.49	30.36	33.09	33.68	33.70
ocean_2kb1	26.83	30.07	15.53	29.70	30.31	30.34	29.94	31.79	21.89	31.60	32.08	32.11
pavia	28.20	31.14	19.67	31.12	31.56	31.58	30.84	32.60	26.99	32.49	32.88	32.90
houston	27.02	30.11	16.67	29.86	30.34	30.37	29.92	31.74	20.91	31.58	31.90	31.92
pleiades1	25.69	28.75	15.07	28.22	28.84	28.87	28.76	30.72	19.29	30.25	30.86	30.92
pleiades2	25.31	28.23	16.68	27.58	28.35	28.38	28.26	30.20	17.40	29.86	30.37	30.39
p160_b_f	21.26	24.29	12.71	24.02	24.55	24.57	24.39	25.81	14.31	25.64	26.03	26.06
Average	24.43	27.63	15.26	27.28	27.81	27.84	27.54	29.18	20.68	28.93	29.37	29.40

Table 4

PSNR (dB) for the proposed CAS-based compression method and other scan-based compression methods.

Image	0.125 bpp						0.5 bpp					
	SPIHT	SPECK	CCSDS	J2K	BTCA	CAS-based	SPIHT	SPECK	CCSDS	J2K	BTCA	CAS-based
europa3	17.45	18.07	16.84	17.92	18.14	18.16	20.95	21.80	20.91	21.59	21.92	21.95
coastal-b1	34.17	35.29	34.28	34.95	35.48	35.51	38.52	39.88	39.06	39.23	40.12	40.15
ocean_2kb1	32.42	33.97	31.14	33.62	34.17	34.20	37.94	39.38	38.93	39.38	39.75	39.77
pavia	33.13	34.34	31.98	34.41	34.62	34.64	37.87	38.88	38.48	39.30	39.35	39.38
houston	32.30	33.57	31.21	33.59	33.86	33.88	37.39	38.51	38.46	38.78	38.93	38.96
pleiades1	31.64	33.26	29.69	33.06	33.64	33.67	38.37	40.62	40.23	40.43	41.40	41.43
pleiades2	31.04	32.72	29.28	32.16	32.94	32.96	37.80	40.03	39.69	39.70	40.32	40.34
p160_b_f	26.49	27.48	21.17	27.37	27.63	27.65	30.65	31.99	31.10	31.77	32.05	32.07
Average	29.83	31.09	28.20	30.89	31.31	31.33	34.94	36.39	35.86	36.27	36.73	36.76

Table 5

PSNR (dB) for the proposed CAS-based compression method and other scan-based compression methods.

Image	1 bpp						1.2 bpp					
	SPIHT	SPECK	CCSDS	J2K	BTCA	CAS-based	SPIHT	SPECK	CCSDS	J2K	BTCA	CAS-based
europa3	23.74	25.37	24.72	25.31	25.46	25.48	25.24	26.54	26.17	26.41	26.69	26.70
coastal-b1	41.51	42.92	41.74	42.01	43.19	43.20	43.06	44.05	42.76	43.04	44.27	44.28
ocean_2kb1	41.59	43.50	43.03	43.61	43.90	43.92	43.60	45.07	44.42	44.99	45.29	45.31
pavia	40.90	42.07	41.84	42.61	42.62	42.66	41.62	43.26	43.15	43.77	43.87	43.88
houston	40.60	41.80	41.85	42.28	42.35	42.36	41.37	43.01	43.22	43.59	43.79	43.81
pleiades1	43.40	45.54	45.36	45.24	45.81	45.83	44.95	46.77	46.67	46.64	47.23	47.25
pleiades2	42.05	44.77	44.86	44.66	45.38	45.40	44.38	46.20	46.15	45.95	46.61	46.62
p160_b_f	33.45	34.71	34.33	34.81	34.95	34.97	34.23	35.86	35.42	36.19	36.08	36.09
Average	38.41	40.09	39.72	40.07	40.46	40.48	39.81	41.35	40.99	41.32	41.73	41.74

Table 6

MAE for the proposed CAS-based compression method and other scan-based compression methods.

Image	0.0313 bpp						0.0625 bpp					
	SPIHT	SPECK	CCSDS	J2K	BTCA	CAS-based	SPIHT	SPECK	CCSDS	J2K	BTCA	CAS-based
europa3	33.05	30.03	68.71	30.56	29.86	29.81	29.37	27.61	36.74	28.21	27.33	27.25
coastal-b1	10.35	4.60	23.78	4.78	4.56	4.49	4.85	3.87	4.98	4.08	3.83	3.75
ocean_2kb1	34.32	23.49	121.43	24.46	22.99	22.87	24.00	19.23	50.58	19.75	18.77	18.62
pavia	51.95	38.42	145.46	37.76	37.38	37.29	39.87	32.44	49.96	33.96	32.41	32.34
houston	61.74	44.39	226.48	45.01	43.66	43.58	44.82	36.83	95.18	37.79	36.65	36.53
pleiades1	159.13	110.84	556.95	119.45	110.39	109.97	110.43	89.31	287.51	92.63	88.15	87.55
pleiades2	168.08	119.10	444.93	127.86	117.73	117.14	118.51	95.72	389.46	98.02	93.93	93.52
p160_b_f	4042.7	3031.8	11424	3045.8	2936.9	2935.1	2895.9	2510.0	8307.4	2548.8	2446.2	2442.9

Table 7

MAE for the proposed CAS-based compression method and other scan-based compression methods.

Image	0.125 bpp						0.5 bpp					
	SPIHT	SPECK	CCSDS	J2K	BTCA	CAS-based	SPIHT	SPECK	CCSDS	J2K	BTCA	CAS-based
europa3	26.49	24.76	27.88	25.04	24.60	24.55	18.01	16.27	17.40	16.45	16.05	16.01
coastal-b1	3.65	3.16	3.46	3.34	3.14	3.05	2.30	2.00	2.09	2.11	1.94	1.82
ocean_2kb1	18.12	15.04	19.28	15.52	14.84	14.80	9.64	8.23	8.33	8.15	8.00	7.76
pavia	31.73	27.95	31.63	27.81	27.53	27.48	19.28	17.48	17.76	16.65	16.86	16.71
houston	34.59	31.12	35.65	30.09	30.08	30.00	20.19	18.10	17.86	17.41	17.54	17.50
pleiades1	79.42	67.62	93.30	67.11	64.42	64.31	37.07	29.33	29.33	29.14	26.81	26.68
pleiades2	85.98	71.84	99.27	74.85	70.62	70.46	39.62	31.01	31.31	31.50	30.41	30.27
p160_b_f	2307.09	2070.7	3388.5	2082.5	2036.2	2030.3	1441.5	1244.2	1360.7	1260.0	1237.2	1235.9

Table 8
MAE for the proposed CAS-based compression method and other scan-based compression methods.

Image	1 bpp						1.2 bpp					
	SPIHT	SPECK	CCSDS	J2K	BTCA	CAS-based	SPIHT	SPECK	CCSDS	J2K	BTCA	CAS-based
europa3	13.07	10.84	11.34	10.71	10.76	10.05	11.01	9.44	9.69	9.48	9.28	9.12
coastal-b1	1.67	1.43	1.56	1.57	1.40	1.26	1.42	1.27	1.40	1.38	1.24	1.16
ocean_2kb1	6.44	5.21	5.26	5.14	5.05	4.86	5.19	4.40	4.52	4.43	4.30	4.19
pavia	14.00	12.45	12.50	11.69	11.80	11.66	13.01	11.11	10.97	10.40	10.43	10.37
houston	14.44	12.76	12.48	12.01	12.13	12.10	13.38	11.37	10.96	10.58	10.47	10.41
pleiades1	21.26	16.91	16.76	17.35	16.40	16.30	17.76	14.47	14.35	14.87	13.86	13.82
pleiades2	24.86	18.53	17.87	18.59	17.25	17.11	18.98	15.50	15.27	16.04	14.90	14.83
p160_b_f	1052.86	915.56	937.26	900.07	890.42	888.82	967.83	807.75	828.34	769.84	789.54	788.53

References

- [1] J.M. Shapiro, Embedded image coding using zerotrees of wavelet coefficients, *IEEE Trans. Signal Process.* 41 (12) (1993) 3445–3462.
- [2] A. Said, W.A. Pearlman, A new, fast, and efficient image codec based on set partitioning in hierarchical trees, *IEEE Trans. Circuits Syst. Video Technol.* 6 (3) (1996) 243–250.
- [3] W.A. Pearlman, A. Islam, N. Nagaraj, A. Said, Efficient low complexity image coding with a set-partitioning embedded block coder, *IEEE Trans. Circuits Syst. Video Technol.* 14 (11) (2004) 1219–1235.
- [4] JPEG2000 Image Coding System, ISO/JEC Std. 15 (444–1) (2000).
- [5] B. Li, R. Yang, H.X. Jiang, Remote-sensing image compression using two-dimensional oriented wavelet transform, *IEEE Trans. Geosci. Remote Sens.* 49 (1) (2011) 236–250.
- [6] A. Karami, M. Yazdi, G. Mercier, Compression of hyperspectral images using discrete wavelet transform and Tucker decomposition, *IEEE J. Sel. Topics Appl. Earth Observ.* 5 (2) (2012) 444–450.
- [7] X. Zhan, R. Zhang, D. Yin, A. Z. Hu, Remote sensing image compression based on double-sparsity dictionary learning and universal trellis coded quantization. in: *Proceedings of the IEEE International Conference of Image Processing*, 2013, pp. 1665–1669.
- [8] C. Jiang, H.Y. zhang, H.F. Shen, L.P. Zhang, Two-step sparse coding for the panning of remote sensing images, *IEEE J. Sel. Topics Appl. Earth Observ.* 7 (5) (2014) 1792–1805.
- [9] J. Xu, H. He, H. Man, DCPE co-training for classification, *Neurocomputing* 86 (2012) 75–85.
- [10] D. Sculley, C. E. Brodley, Compression and machine learning: A new perspective on feature space vectors. In: *Proceedings of the Data Compression Conference*, 2006, pp. 332–341.
- [11] A. Montalto, G. Tossatore, R. Prevete, A linear approach for sparse coding by a two-layer neural network, *Neurocomputing* 149 (2015) 1315–1323.
- [12] A.J. Hussain, D. Jumeily, N. Radi, P. Lisboa, Hybrid neural network predictive-wavelet image compression system, *Neurocomputing* 151 (2015) 975–984.
- [13] E. Magli, G. Olmo, E. Quacchio, Optimized onboard lossless and near-lossless compression of hyperspectral data using CALIC, *IEEE Lett. Geosci. Remote Sens.* 1 (1) (2004) 21–25.
- [14] F. García-Vilchez, J. Serra-Sagrà, Extending the CCSDS recommendation for image data compression for remote sensing scenarios, *IEEE Trans. Geosci. Remote Sens.* 47 (10) (2009) 3431–3445.
- [15] P. Corsonello, S. Perri, G. Staino, M. Lanuzza, G. Cocorullo, Low bit rate image compression core for onboard space applications, *IEEE Trans. Circuits Syst. Video Technol.* 16 (1) (2006) 114–128.
- [16] S.E. Qian, M. Bergeron, I. Cunningham, L. Gagnon, A. Hollinger, Near lossless data compression onboard a hyperspectral satellite, *IEEE Trans. Aerosp. Electron. Syst.* 42 (3) (2006) 851–866.
- [17] A. Abrardo, M. Barni, E. Magli, F. Nencini, Error-resilient and low-complexity onboard lossless compression of hyperspectral images by means of distributed source coding, *IEEE Trans. Geosci. Remote Sens.* 48 (4) (2010) 1892–1904.
- [18] S. Wang, L. Cui, S. Cheng, L.S. tankovic, V. Stankovic, Onboard low-complexity compression of solar stereo images, *IEEE Trans. Image Process.* 21 (6) (2012) 3114–3118.
- [19] D. Valsesia, E. Magli, A novel rate control algorithm for onboard predictive coding of multispectral and hyperspectral images, *IEEE Trans. Geosci. Remote Sens.* 52 (10) (2014) 6341–6355.
- [20] K. Huang, D. Dai, A new on-board image codec based on binary tree with adaptive scanning order in scan-based mode, *IEEE Trans. Geosci. Remote Sens.* 50 (10) (2012) 3737–3750.
- [21] P. Kulkarni, A. Bilgin, M.W. Marcellin, J.C. Dagher, J.H. Kasner, T.J. Flohr, J. C. Rountree, B. Du, Compression of earth science data with JPEG2000, *Hyperspectr. Data Compress.* (2006) 347–378.
- [22] CCSDS122.0-B-1, Image Data Compression, Nov. 2005. [Online]. Available: (<http://public.ccsds.org/publications/archive/122x0b1c3.pdf>).
- [23] CCSDS120.1-G-1, Image Data Compression, Jun. 2007. [Online]. Available: (<http://public.ccsds.org/publications/archive/120x1g1e1.pdf>).
- [24] L. Zhang, L. Zhang, D. Tao, X. Huang, Compression of hyperspectral remote sensing images by tensor approach, *Neurocomputing* 147 (2015) 358–363.
- [25] E. Magli, Multiband lossless compression of hyperspectral images, *IEEE Trans. Geosci. Remote Sens.* 47 (4) (2009) 1168–1178.
- [26] X. Pan, R. Liu, X.Q. Lv, Low-complexity compression method for hyperspectral images based on distributed source coding, *IEEE Geosci. Remote Sens. Lett.* 9 (2) (2012) 224–227.
- [27] B. Aiazzi, L. Alparone, S. Baronti, C. Lastrì, Crisp and fuzzy adaptive spectral predictions for lossless and near-lossless compression of hyperspectral imagery, *IEEE Lett. Geosci. Remote Sens.* 4 (4) (2007) 532–536.
- [28] X. Hou, J. Yang, G. Jiang, X. Qian, Complex SAR image compression based on directional lifting wavelet transform with high clustering capability, *IEEE Trans. Geosci. Remote Sens.* 51 (1) (2013) 527–538.
- [29] G. Dua, R. Mulaveesala, Applications of Barker coded infrared imaging method for characterisation of glass fibre reinforced plastic materials, *Electron. Lett.* 49 (17) (2013) 1071–1073.
- [30] N. Memon, D.L. Neuhoff, S. Shende, An analysis of some common scanning techniques for lossless image coding, *IEEE Trans. Image Process.* 9 (11) (2000) 1837–1848.
- [31] X. Wu, N. Memon, Context-based, adaptive, lossless image coding, *IEEE Trans. Commun.* 45 (4) (1997) 437–444.
- [32] C.A. Shaffer, R. Juvvadi, L.S. Health, Generalized comparison of quadtree and bintree storage requirements, *Image and Vision Computing* 11 (7) (1993) 402–412.
- [33] CCSDS reference test image set, Apr.2007. [Online]. Available: (<http://cwe.ccsds.org/sls/docs/sls-dc/>).



Cuiping Shi received the B.S. degree from the Daqing petroleum Institute, Daqing, China, in 2004 and the M.S. degree from the Yangzhou University, Yangzhou, China, in 2007. Currently, she is pursuing Ph.D. degree in signal and information processing from the Harbin Institute of Technology (HIT). Her research fields include remote sensing image processing and compression.



Junping Zhang received the B.S. degree in biomedical engineering from Harbin Engineering University, in 1993 and the M.S. and Ph.D. degrees in signal and information processing from the Harbin Institute of Technology (HIT), in 1998 and 2002, respectively. Between 2011 and 2012, she was a Visiting Scholar in the University of Michigan State University, USA. She is currently a professor with the Department of Information Engineering, HIT. She is the author or co-author of more than 70 papers. Her research interests include remote sensing image processing, image compression, multisource information fusion.



Ye Zhang received the B.S., M.S., and Ph.D. degrees from the Harbin Institute of Technology (HIT), China, in 1982, 1985, and 1996, respectively. He is currently a Professor of the Department of Information Engineering, HIT. Between 1998 and 1999, he was a Visiting Scholar in the University of Texas at San Antonio, USA. He was responsible for, or participated in more than 30 research projects which are the National Natural Science Foundation of China, 863 projects, etc. He is the author or co-author of more than 200 papers and has written three books. His main research interests include hyperspectral image analysis and processing, image and video compression and transmission, and multisensor-based remote sensing image applications.

2原件

WEB OF SCIENCE™

检索 返回检索结果

我的工具 | 检索历史 | 标记结果列表

全文选项 | 查找全文 | 保存至 EndNote online | 添加到标记结果列表

第 1 条, 共 1 条

Content-based onboard compression for remote sensing images

作者: Shi, CP (Shi, Cuiping)^{1,2,1}; Zhang, JP (Zhang, Junping)^{1,1}; Zhang, Y (Zhang, Ye)^{1,1}

NEUROCOMPUTING

卷: 191 页: 330-340

DOI: 10.1016/j.neucom.2016.01.048

出版年: MAY 26 2016

查看期刊信息

摘要

New-generation instruments on spacecraft are collecting a large amount of information at an increasing rate, which makes the onboard data compression a challenging task. Moreover, existing compression methods usually scan an image in a fixed way without considering the content of the image, which makes the performance improvements of these methods often marginal at best. In this paper, we present a novel, content-based, adaptive scanning (CAS) scheme for onboard compression. For a remote sensing image, first, the wavelet transform is performed. Second, an adaptive scanning method is proposed, which can provide different scanning orders among and within subbands, respectively. The former aims at organizing the codestream according to the importance of subbands, and the latter focuses on preserving the texture information as much as possible. Finally, the binary tree codec is utilized to code the 1-D coefficient array after scanning. Experimental results demonstrate that compared with other scan based compression methods, including CCSDS, JPEG2000, and even the state-of-the-art adaptive binary tree coding (BTCA), the proposed compression method can effectively improve the coding performance. In addition, the method does not use entropy coding or any complicated components, which makes it extremely suitable for onboard compression. © 2016 Elsevier B.V. All rights reserved.

关键词

作者关键词: Onboard compression; Content-based; Adaptive scanning; Remote sensing image; Binary tree coding

KeyWords Plus: NEAR-LOSSLESS COMPRESSION; HYPERSPECTRAL IMAGES; WAVELET TRANSFORM; NEURAL-NETWORK; EFFICIENT

作者信息

通讯作者地址: Zhang, JP (通讯作者)

+ Harbin Inst Technol, Dept Informat Engn, Harbin 150001, Peoples R China

地址:

+ [1] Harbin Inst Technol, Dept Informat Engn, Harbin 150001, Peoples R China

+ [2] Qiqihar Univ, Dept Commun Engn, Qiqihar 161000, Peoples R China

基金资助致谢

基金资助机构	授权号
National Natural Science Foundation of China	61271348
Prophase Cultivation Project of Technology Achievements Industrialization of Universities in Heilongjiang Province of China	1254CGZH04

查看基金资助信息

出版商

ELSEVIER SCIENCE BV, PO BOX 211, 1000 AE AMSTERDAM, NETHERLANDS

类别 / 分类

研究方向: Computer Science

引文网络

0 被引频次

33 引用的参考文献

查看 Related Records

查看引证关系图

创建引文跟踪

在数据库中检索 Web of Science™ 核心合集

全部被引频次计数

0 / 所有数据库

0 / Web of Science 核心合集

0 / BIOSIS Citation Index

0 / 中国科学引文数据库

0 / Data Citation Index

0 / Russian Science Citation Index

0 / ScELO Citation Index

使用次数

最近 180 天: 9

2013 年至今: 9

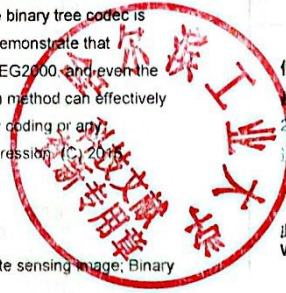
进一步了解

此记录来自:

Web of Science™ 核心合集

建议修正

如果您希望提高此记录中数据的质量, 请提供修正建议。



文献信息

文献类型: Article

语种: English

入藏号: WOS 000375165900027

ISSN: 0925-2312

eISSN: 1872-8286

期刊信息

Impact Factor (影响因子): Journal Citation Reports®

其他信息

IDS号: DK8GT

Web of Science 核心合集中的“引用的参考文献”: 33

Web of Science 核心合集中的“被引频次”: 0



第 1 条, 共 1 条